A Shared-Aperture Decoupling Network (SADN) for Dual-Band Differentially-Fed Antenna (DFA) Array

Xichen Wang[1], Can Ding[2], Shiyong Li[1,3], Guoqiang Zhao[1,3], Houjun Sun[1,3]
[1] The Beijing Key Laboratory of Millimeter Wave and Terahertz Technology, Beijing Institute of Technology (BIT), Beijing, China, wangxichen000512@163.com
[2] The Global Big Data Technologies Center, University of Technology Sydney (UTS), NSW, Australia, can.ding@uts.edu.au
[3] The Tangshan Research Institute, Beijing Institute of Technology (BIT), Tangshan, China, lishiyong@bit.edu.cn

***Abstract*—This paper proposes a dual-band shared-aperture decoupling network (SADN) to suppress mutual coupling in a dual-band antenna array. The array consists of two high-band (HB) patches and two low-band (LB) patches, all fed differentially. The SADN addresses both in-band coupling between the two HB antennas and between the two LB antennas, as well as cross-band coupling between the LB and HB antennas. The SADN can adapt to multi-band DFA arrays with different frequency ratios. To validate the design principle, a dual-band DFA array operating at 18.5 GHz and 28 GHz with a frequency ratio of 1:1.51 was designed, fabricated, and tested. The fractional bandwidths of the two bands are 5.4% and 10.1%, respectively. Within both bands, the isolation between any ports exceeds 26 dB. Compared to the case without the SADN, significant isolation improvements ranging from 15 dB to 45 dB have been achieved.**

***Index Terms*—antenna decoupling, differentially-fed antenna (DFA), dual-band antenna array, shared-aperture antenna, shared-aperture decoupling network (SADN)**

I. Introduction

Recently, due to their balanced symmetrical structure and excellent anti-interference capabilities [1]-[2], research on differentially-fed antennas (DFAs) has been gaining momentum, with most efforts focusing on broadening impedance bandwidth [3]-[4]. However, when DFA elements are extended into tightly arranged arrays, mutual coupling among them must be carefully considered to prevent performance deterioration. Despite extensive research efforts on antenna decoupling, few studies have focused on DFAs. Existing decoupling methods for single-fed antennas (SFAs) can be applied to DFAs, but they often compromise structural symmetry, negating the advantages of DFAs. In 2024, a few decoupling methods specifically designed for DFAs were developed [5]-[6], but they feature very narrow bandwidths (less than 3%).

Concurrently, as wireless communication technology advances, the electromagnetic spectrum is becoming increasingly congested. In response to this challenge, multi-band shared-aperture antennas [7]-[17] have emerged as effective solutions. Multiple antennas operating at different frequency bands are typically arranged in various configurations, such as stacked [7]-[9], interleaved [10]-[15], or embedded schemes [16]-[17], to achieve multi-band operation within a compact size. The close proximity of collocated antennas operating at different frequency bands makes decoupling more challenging, as both in-band coupling between antennas at the same frequency and cross-band coupling between antennas at different frequencies must be addressed.

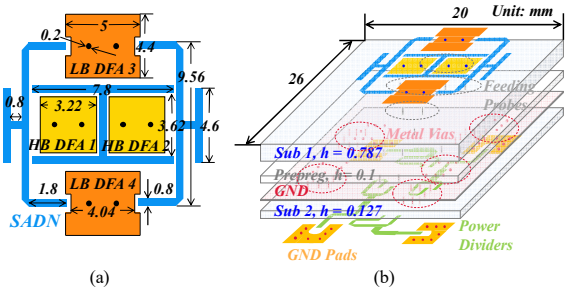

Fig. 1. (a) Perspective view and (b) top view of the dual-band shared-aperture DFA array decoupled by a dual-band shared-aperture decoupling network (SADN).

Addressing the coupling among DFAs is more challenging than for SFAs. Firstly, the coupling conditions among DFAs are more complex due to the greater number of feeding ports compared to SFAs. Secondly, the decoupling structure must remain symmetric; otherwise, the DFAs will lose the symmetry that gives them their inherent advantages over SFAs. Thirdly, the feed network of a DFA is more intricate than that of SFAs. This is especially true for multi-band shared-aperture DFAs, where the space to accommodate both decoupling and feed networks is more constrained.

In this paper, a shared-aperture decoupling network (SADN) is proposed to significantly improve isolation in a dual-band DFA array with a frequency ratio of 1:1.51, as shown in Fig. 1. The two LB DFAs, two HB DFAs, and the SADN are collocated on a single layer, i.e., the top side of Substrate 1. The bottom layer houses four differential power dividers, which are used mainly for providing differential feeding. The two HB DFAs operate in the frequency band from 26.93 to 29.75 GHz, with a fractional bandwidth of 10.1%, while the two LB DFAs operate in the band from 17.75 to 18.84 GHz, with a fractional bandwidth of 5.4%. All the DFAs are horizontally polarized. The isolation improvements achieved by the SADN are as high as 42 dB for in-band isolation and 25 dB for cross-band isolation at the center frequencies. At both frequency bands, the isolation between any two of the four antennas is greater than 26 dB.

II. SINGLE-BAND DFA DECOUPLING

The design begins with decoupling two closely spaced HB DFAs. As shown in Fig. 2, a single-band decoupling network (DN) consisting of an H-shaped strip and a pair of bracket strips are employed to decouple the two DFAs. When DFA 1 is excited, generating currents I^E, it couples to DFA 2, inducing a current I^C. The DN introduces a new coupling path, inducing horizontal currents I^D and vertical currents on DFA 2. Due to the symmetrical structure, the vertical currents can cancel each other in vertical direction. For the horizontal currents on DFAs, by optimizing the parasitic strips to ensure $I^D + I^C = 0$, decoupling can be achieved. Although this concept is widely known and effective, to achieve this condition across a wide band is challenging. To enhance the decoupling bandwidth, we adopt a different strategy specifically designed for DFAs.

Fig. 3(a) shows the current distributions of two coupled DFAs without the DN when the left DFA is excited. Significant coupling currents are observed, with the magnitude of the coupling currents near the left port being noticeably higher than near the right port. This occurs because the coupled antenna has two ports, and the distances between each port and the excited antenna differ. This coupling imbalance between the two ports presents an additional challenge when addressing decoupling.

Traditional decoupling aims to zero the induced currents on the feed ports of the coupled antenna, i.e., $I_{P2+} = 0$ and $I_{P2-} = 0$. However, since the two ports (P2+ and P2-) are later combined with a 180-degree phase difference, it is only necessary to ensure that $I_{P2+} = I_{P2-}$, rather than making the currents at each port zero. This relaxed condition enables the possibility of achieving wideband decoupling using a simple method.

Fig. 3(b) presents the current distributions of the two DFAs with the DN. After adding the DN, the current density on the coupled patch is reduced across all the sampled frequencies. However, some residual currents are still visible near the ports, i.e., $I_{P2+} \neq 0$ and $I_{P2-} \neq 0$.

Fig. 4(a) compares the transmission coefficients between the two DFAs without and with the DN. Without the DN, the isolation is only around 12 dB. Once the DN is employed, the isolation is significantly enhanced, despite the residual currents shown in Fig. 3(b). To better understand this improvement, Fig. 4(b) compares the transmission coefficients without and with the DN, between the left DFA (excited as a whole antenna using a differential power divider) and the two separate ports (P2+ and P2-) of the right DFA. It is observed that, with the DN, the power entering P2+ and P2- differs significantly, reflecting the results seen in Fig. 3(a). After adding the DN, the transmission coefficients range from -20 to -30 dB, indicating that the power entering the two ports (P2+ and P2-) is reduced. More importantly, the magnitudes of the power entering the two ports are brought to similar levels, resulting in an even lower overall power level after summing them up, with transmission coefficients dropping below -50 dB at 28 GHz, as shown in Fig. 4(a).

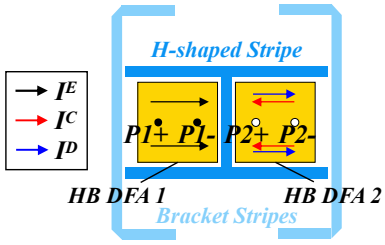

Fig. 2. Configuration of the HB DFAs decoupled by the single-band decoupling network (DN) and illustration of the current distributions on the decoupled HB DFAs.

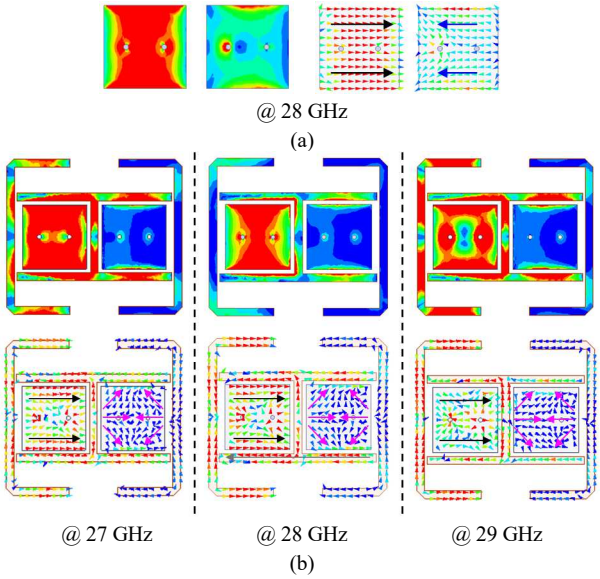

Fig. 3. Current distributions in both magnitude and vector forms for (a) the two coupled DFAs at 28 GHz and (b) the decoupled DFAs with SADN at 27 GHz, 28 GHz, and 29 GHz.

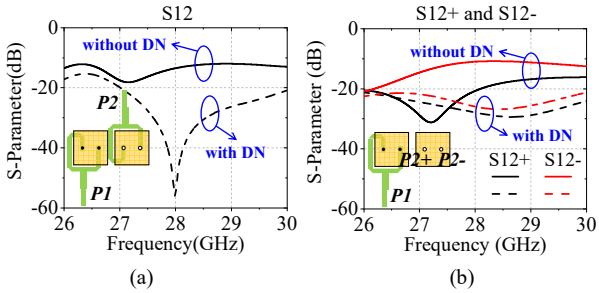

Fig. 4. Comparison of the transmission coefficients between the two DFAs without and with the SADN: (a) S12. (b) S12+ and S12-.

It is also worth mentioning that the coupling mitigation is mainly achieved by the H-shaped parasitic strip. However, as shown in Fig. 3(b), vertical currents are introduced on both the DFA and the decoupling structure, which can reduce gain. The two bracket stripes help alleviate gain reduction by introducing reversed induced currents in the vertical direction. The simulated realized gain improves from 5.3 dBi to 6.6 dBi after loading the bracket stripes.

III. DUAL-BAND DFA DECOUPLING

Fig. 5 shows the configuration of the dual-band shared-aperture DFA array decoupled by the dual-band SADN. The two LB DFAs are arranged at the top and bottom of the HB DFA array, with an edge-to-edge distance of 0.67 mm, which corresponds to only 0.04 wavelength at the lower center frequency of 18.5 GHz. Compared to the single-band DN configuration shown in Fig. 2, only two additional T-shaped strips are added to form the final dual-band SADN. The goal here is to achieve decoupling for the two LB DFAs while maintaining the decoupling effect for the two HB DFAs.

The presence of the LB DFAs and the two T-shaped strips can be viewed as a slight modification of the original single-band DN. Therefore, by adjusting the dimensions of the strips, the decoupling of the two HB DFAs can be preserved. For the decoupling of the two LB DFAs, to avoid introducing excessive complexity, we primarily optimize the bracket strips and the T-shaped strips. The H-shaped strip and the two HB DFAs are treated as a single parasitic element and are not optimized.

Fig. 5 also presents the equivalent circuits of the decoupling structure for the LB DFAs. Z_1 and Z_2, as well as θ_1 and θ_2 represent the impedance and electrical length of the transmission lines (bracket and T-shaped strips). Cs denotes the coupling capacitance between the decoupling strips and the LB DFAs. The transfer matrix T_C between DFAs 3 and 4 can be obtained through full-wave simulation. After decoupling the HB DFA array, the values of Cs, Z_1 and θ_1 are determined. The coupling can be effectively suppressed by inserting stripes with an impedance of Z_2. High isolation is achieved by adjusting the values of Z_2 and θ_2. The matrix analysis follows a similar approach to our previous work [5] but also incorporates the new strategy described in Section II to improve bandwidth.

To illustrate the decoupling performance, Fig. 6 compares the current distributions on the array without and with the SADN at 18.5 GHz. The in-band and cross-band transmission coefficients between the four antennas are presented in Fig. 7 for both cases. It is evident that, when the top LB DFA is excited, the SADN significantly reduces the coupled currents on the other LB DFA. Additionally, it suppresses cross-band coupling, as shown by the much lower current density on the HB DFAs. The detailed working mechanisms are not elaborated here due to space constraints.

Fig. 7 compares the simulated transmission coefficients with and without the SADN to evaluate the decoupling performance. Significant improvements have been achieved for both in-band and cross-band isolations. The improvement reaches up to 48 dB at the LB center frequency and 42 dB at the HB center frequency.

IV. RESULTS

The dual-band DFA array with the SADN was also fabricated and measured. Fig. 8 presents the top view and bottom view of the fabricated prototype. The simulated and measured S-parameters of the dual-band DFA array are plotted in Fig. 9. As shown in Fig. 9(a), the measured

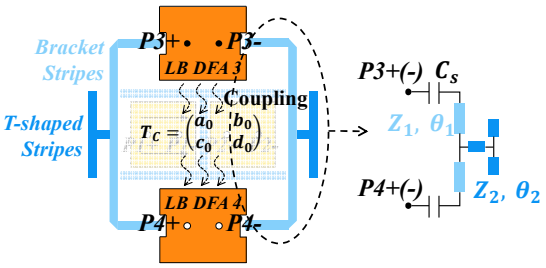

Fig. 5. Configuration of the dual-band DFA array decoupled by the SADN and illustration of the decoupling mechanism.

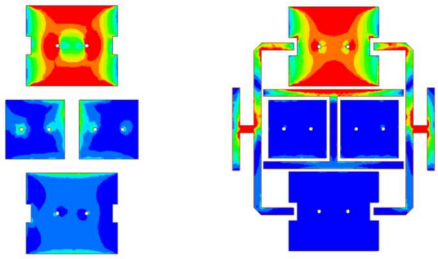

(a) (b)

Fig. 6. Current distributions on the dual-band shared-aperture antenna array (a) without and (b) with the SADN.

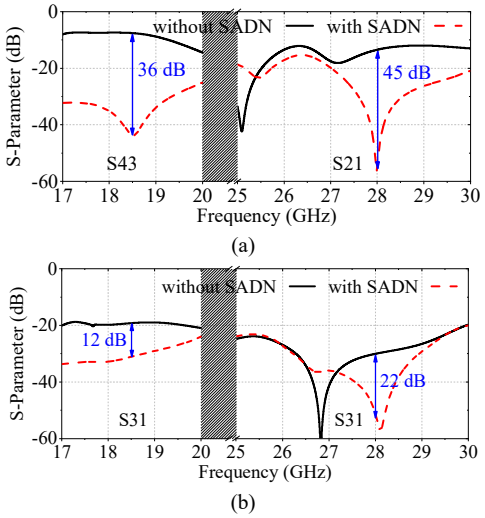

Fig. 7. Comparison of the simulated (a) in-band transmission coefficients and (b) cross-band transmission coefficients among the dual-band shared-aperture DFA array without and with the SADN.

reflection coefficients shift towards lower frequencies compared to the simulated results for both the LB DFA and HB DFAs. For clarity, only S11 and S33 are shown, as S22 and S44 exhibit similar characteristics due to structural symmetry. According to the measured results, the impedance matching bandwidths are 17.7 to 18.8 GHz (5.4%) for the LB and 26.93 to 29.75 GHz (10.1%) for the HB.

Figs. 9(b) and 9(c) present the simulated and measured results of the in-band coupling and cross-band coupling, respectively. Overall, the measurements agree well with the simulations. According to Fig. 9(b), the highest isolation achieved between the two LB antennas is 53 dB, remaining above 35 dB across the entire LB band. For the in-band

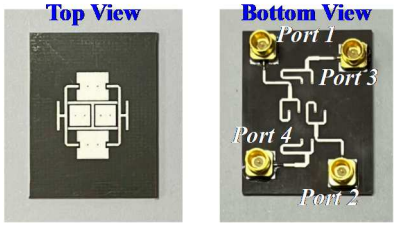

Fig. 8. Fabricated prototype of the dual-band DFA array with SADN.

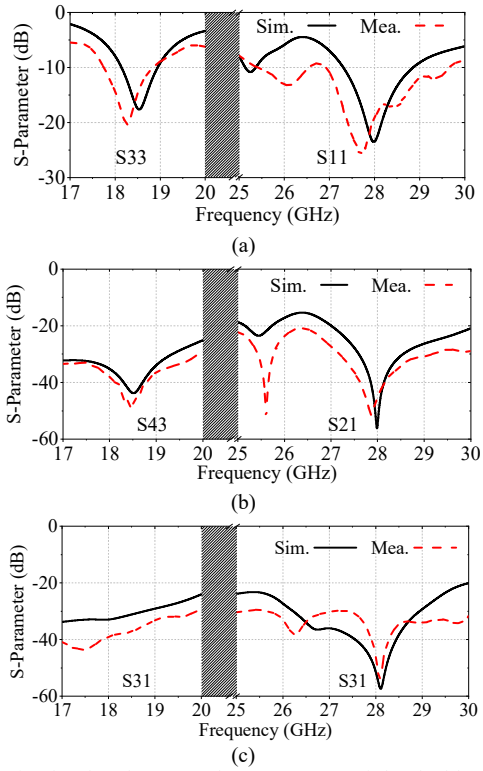

Fig. 9. Simulated and measured S-parameters of the dual-band DFA array with SADN. (a) Reflection coefficients of HB DFA1 and LB DFA3. (b) In-band transmission coefficients between the two LB antennas and two HB antennas. (c) Cross-band transmission coefficients between HB DFA1 and LB DFA3.

isolation between the two HB antennas, it reaches 52 dB near 28 GHz and stays above 26 dB across the entire HB band. As shown in Fig. 9(c), the cross-band isolations between the LB and HB ports across both operating bands are greater than 30 dB.

The simulated and measured radiation patterns of the decoupled dual-band DFA array are depicted in Fig. 10. Fig. 10(a) shows the E- and H-plane patterns at the LB frequency of 18.5 GHz, while Fig. 10(b) presents the patterns at three HB frequencies. The measured results align well with the simulations. It is worth mentioning that the symmetry of the HB patterns in the H-plane is slightly deteriorated, primarily due to residual currents on the coupled antenna and the contribution of the currents on the bracket strips, which is a limitation of this decoupling method. Nevertheless, the cross-polarization levels remain quite low, demonstrating

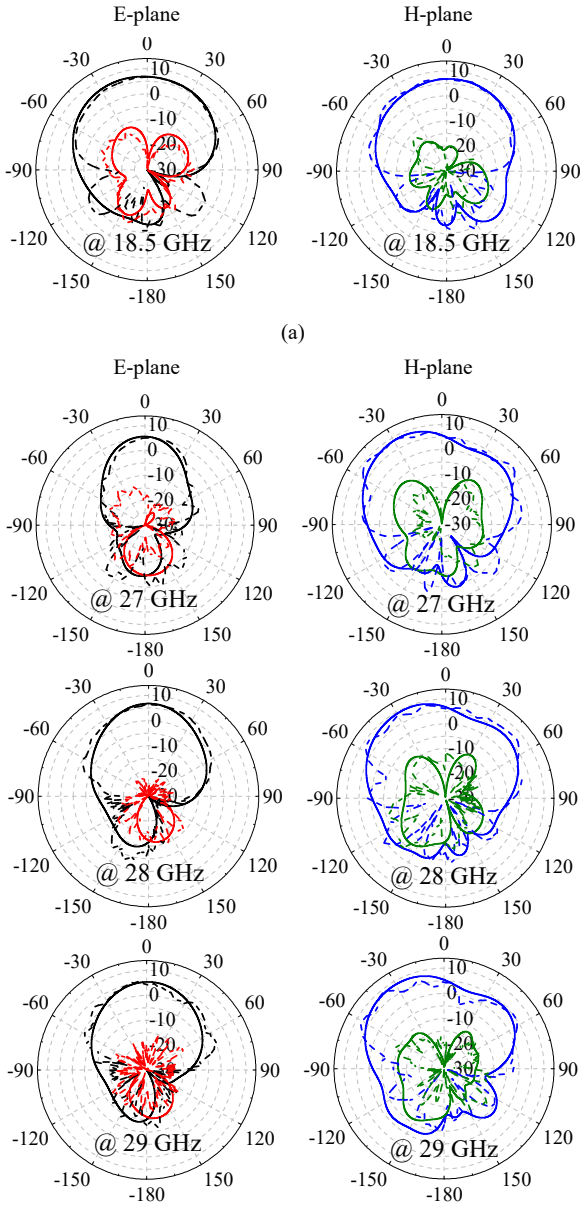

Fig. 10. Simulated and measured radiation patterns of (a) the LB DFA and (b) the HB DFA in both the E- and H-planes. (Solid lines denote the simulated results, and dashed lines represent the measured results.)

that the decoupled DFAs retain their original advantages over SFAs due to the preserved structural symmetry.

To demonstrate the superior performance of the proposed SADN, a comparison with state-of-the-art decoupling methods is presented in TABLE I. Only a few decoupling methods have been specifically designed for DFAs, and they are all single-band antennas. Compared to those designs, our approach achieves a much wider decoupling bandwidth. There are also several multi-band shared-aperture antenna designs. However, the decoupling methods used in these works typically address only a few types of coupling, resulting in limited isolation improvements. In contrast, the SADN

TABLE I. THE COMPARISON OF THE DECOUPLING PERFORMANCE

Ref.	Bands	Feed Type	Method	f_c (GHz)	ES	Bandwidth	Isolation (dB)		Isolation Improvement (dB)	
							in BW	At f_c	in BW	At f_c
[1]	Single-Band	DFA	DSDN	2.45	0.08 λ	1.2%	> 18	65	6	53
[2]			Self-Decoupling	5.9	0.37 λ	2.9%	> 35	36	18	18
[7]	Multi-Band Shared-Aperture	SFA	Stripe+MS	f_L: 0.9 f_M: 1.8 f_H: 3.5	0.17 λ_L 0.33 λ_M 0.7 λ_H	L: 8.8% M: 9.4% H: 5.7%	L: > 28 H: > 18	L: 29 M: 30	L: No M: 7 H: No	L: No M: 11 H: No
[8]			Self-Decoupling	f_L: 1.9 f_H: 3.5	0.69 λ_H	L: 15.6% H: 7.7%	L: No H: > 27	L: No H: 38.6	L: No H: 9	L: No H: 18
[9]			Path-Extension	f_L: 0.86 f_M: 1.9 f_H: 3.5	0.5 λ_L 0.35 λ_M 0.64 λ_H	L: 19.8% M: 24.2% H: 5.7%	L: > 28 M: > 25 H: > 20	L: 30 M: 30 H: 26	L: 6 M: No H: No	L: 10 M: No H: No
[12]			DBL	f_L: 2.2 f_H: 3.6	0.5 λ_H	L: 27% H: 16.7%	L: No H: > 25	L: No H: 38	L: No H: 8	L: No H: 18
Our Work		**DFA**	**SADN**	**f_L: 18.5 f_H: 28**	**0.7 λ_L 0.07 λ_H**	**L: 5.4% H: 10.1%**	**L: > 35 H: > 26 Cx: > 30**	**L: 50 H: 53 Cx: 55**	**L: >27 H: >18 Cx: >12**	**L: 42 H: 45 Cx: 22**

significantly enhances both in-band isolation and cross-band isolation at both the LB and HB frequencies.

V. CONCLUSION

This work proposes a novel and simple method specifically for decoupling DFAs. Instead of completely eliminating the coupling currents entering the ports of the coupled antenna, this approach allows for residual currents. The decoupling network ensures that the currents entering the two differential ports are equal, thus canceling each other out due to the differential feeding. This new approach improves the decoupling bandwidth compared to previous methods. Then, two pairs of DFAs operating at different frequency bands are collocated to achieve multi-band operation in a compact size. A dual-band shared-aperture decoupling network (SADN) is developed, which significantly reduces both in-band and cross-band coupling within the array. Unlike the strategies in other shared-aperture antenna designs that primarily focus on sharing the aperture between radiators and/or feeding networks, this work introduces a novel approach where both the decoupling networks and radiators share the aperture. This provides an integrated and efficient solution for multi-band decoupling.

REFERENCES

[1] T. Brauner, R. Vogt, and W. Bachtold, “A differential active patch antenna element for array applications,” *IEEE T. Microw. Wireless* Comp. Lett., vol. 13, no. 4, pp. 161–163, 2003.

[2] A. R. Behzad et al., “A 5-GHz direct-conversion CMOS transceiver utilizing automatic frequency control for the IEEE 802.11a wireless LAN standard,” IEEE J. Solid-State Circuits, vol. 38, no. 12, pp. 2209–2220, Dec. 2003.

[3] M. Wang and C. H. Chan, "A Novel Differentially-Fed Dual-Polarized Shared Aperture Antenna Array," *IEEE Trans. Antennas Propag.*, vol. 70, no. 12, pp. 12276-12281, Dec. 2022

[4] Y. Hou, Y. Zhang and J. Mao, "A Differential Wideband Circularly Polarized Laminated Resonator Antenna," *IEEE Antennas Wireless Propag. Lett.*, vol. 22, no. 2, pp. 278-282, Feb. 2023

[5] X. Wang, C. Ding, G. Zhao, S. Li, Y. Chen and H. Sun, "Differential and Symmetrical Decoupling Network for Differentially Fed Antennas," *IEEE Antennas Wireless Propag. Lett.*, vol. 23, no. 3, pp. 1129-1133, March 2024.

[6] J. Xu, X. He and T. Deng, "A Self-Decoupled MIMO Patch Array with Consistent Radiation Patterns," *IEEE Trans. Antennas Propag.*

[7] H. Huang, X. Li and Y. Liu, "A Way to Improve Mutual Isolation and Radiation Pattern of Triple-Band Antenna," *IEEE Antennas Wireless Propag. Lett.,* vol. 21, no. 7, pp. 1433-1436, July 2022.

[8] Y. Li and Q. -X. Chu, "Self-Decoupled Dual-Band Shared-Aperture Base Station Antenna Array," *IEEE Trans. Antennas Propag.*, vol. 70, no. 7, pp. 6024-6029, July 2022.

[9] Y. -L. Chang and Q. -X. Chu, "Suppression of Cross-Band Coupling Interference in Tri-Band Shared-Aperture Base Station Antenna," *IEEE Trans. Antennas Propag.*, vol. 70, no. 6, pp. 4200-4214, June 2022.

[10] H. Huang, “A decoupling method for antennas with different frequencies in 5G massive MIMO application,” *IEEE Access*, vol. 8, pp. 140273–140278, 2020.

[11] X. Liu et al., "A Mutual-Coupling-Suppressed Dual-Band Dual-Polarized Base Station Antenna Using Multiple Folded-Dipole Antenna," *IEEE Trans. Antennas Propag.*, vol. 70, no. 12, pp. 11582-11594, Dec. 2022.

[12] Y. Da, X. Chen and A. A. Kishk, "In-Band Mutual Coupling Suppression in Dual-Band Shared-Aperture Base Station Arrays Using Dielectric Block Loading," *IEEE Trans. Antennas Propag.*, vol. 70, no. 10, pp. 9270-9281, Oct. 2022.

[13] H. Yuan, F. -C. Chen, W. -F. Zeng and Q. -X. Chu, "Dual-Band Base Station Antenna Array with Cross-Band Scattering and In-Band Coupling Suppression," *IEEE Trans. Antennas Propag.*, vol. 71, no. 5, pp. 3983-3991, May 2023.

[14] S. -Y. Sun, C. Ding, W. Jiang and Y. J. Guo, "Simultaneous Suppression of Cross-Band Scattering and Coupling Between Closely Spaced Dual-Band Dual-Polarized Antennas," *IEEE Trans. Antennas Propag.*, vol. 71, no. 8, pp. 6423-6434, Aug. 2023.

[15] H. Sun, C. Ding, H. Zhu, B. Jones and Y. J. Guo, "Suppression of cross-band scattering in multiband antenna arrays", *IEEE Trans. Antennas Propag.*, vol. 67, no. 4, pp. 2379-2389, Apr. 2019.

[16] L. Y. Nie et al., “A low-profile coplanar dual-polarized and dual-band base station antenna array,” *IEEE Trans. Antennas Propag.*, vol. 66, no. 12, pp. 6921–6929, Dec. 2018.

[17] Y. Liu, S. Wang, N. Li, J.-B. Wang, and J. Zhao, “A compact dualband dual-polarized antenna with filtering structures for sub-6 GHz base station applications,” *IEEE Antennas Wireless Propag.* Lett., vol. 17, no. 10, pp. 1764–1768, Oct. 2018.